Acta Pharmacologica Sinica

www.nature.com/aps

ARTICLE

Aiphanol, a multi-targeting stilbenolignan, potently suppresses mouse lymphangiogenesis and lymphatic metastasis

Shan-mei Chen[1], Chuan-ke Zhao[1], Li-cheng Yao[2], Li-xin Wang[1], Yu-nan Ma[3], Lin Meng[1], Shao-qing Cai[2], Cai-yun Liu[1], Li-ke Qu[1], Yan-xing Jia[2] and Cheng-chao Shou[1]

The high incidence of lymphatic metastasis is closely related to poor prognosis and mortality in cancers. Potent inhibitors to prevent pathological lymphangiogenesis and lymphatic spread are urgently needed. The VEGF-C-VEGFR3 pathway plays a vital role in driving lymphangiogenesis and lymph node metastasis. In addition, COX2 in tumor cells and tumor-associated macrophages (TAMs) facilitates lymphangiogenesis. We recently reported that aiphanol, a natural stilbenolignan, attenuates tumor angiogenesis by repressing VEGFR2 and COX2. In this study, we evaluated the antilymphangiogenic and antimetastatic potency of aiphanol using in vitro, ex vivo and in vivo systems. We first demonstrated that aiphanol directly bound to VEGFR3 and blocked its kinase activity with an half-maximal inhibitory concentration (IC_{50}) value of 0.29 μM in an in vitro ADP-Glo^{TM} kinase assay. Furthermore, we showed that aiphanol (7.5−30 μM) dose-dependently counteracted VEGF-C-induced proliferation, migration and tubular formation of lymphatic endothelial cells (LECs), which was further verified in vivo. VEGFR3 knockdown markedly mitigated the inhibitory potency of aiphanol on lymphangiogenesis. In 4T1-luc breast tumor-bearing mice, oral administration of aiphanol (5 and 30 $mg \cdot kg^{-1} \cdot d^{-1}$) dose-dependently decreased lymphatic metastasis and prolonged survival time, which was associated with impaired lymphangiogenesis, angiogenesis and, interestingly, macrophage infiltration. In addition, we found that aiphanol decreased the COX2-dependent secretion of PGE2 and VEGF-C from tumor cells and macrophages. These results demonstrate that aiphanol is an appealing agent for preventing lymphangiogenesis and lymphatic dissemination by synergistically targeting VEGFR3 and inhibiting the COX2-PGE2-VEGF-C signaling axis.

Keywords: aiphanol; SAR131675; lymphangiogenesis; lymphatic metastasis; VEGFR3; COX2

Acta Pharmacologica Sinica (2023) 44:189–200; https://doi.org/10.1038/s41401-022-00940-4

INTRODUCTION

Previous studies have shown that metastasis is responsible for 90% of cancer-related deaths worldwide, however, effective therapeutic drugs are scarce [1]. Lymphatic metastasis is the process by which tumor cells invade along lymphatic vessels at the early stage which enhances devastating dissemination into peripheral tissues and subsequently to distant sites. Clinical evidence disclosed that the contribution of lymphatic vessels to mediate cancer cell dissemination is 3–5 times higher than that of blood vessels, a phenomenon that can be attributed to the lymphatic dilation that facilitates the intravasation and extravasation of tumor cells and benefits their survival in the lymphatic system [2]. Thus, lymphatic vessels have emerged as important targets for the development of strategies to treat metastasis.

The growth of lymphatic vessels (lymphangiogenesis) is uncommon in healthy adults, but is elicited in diverse pathological conditions, such as inflammatory diseases and cancer metastasis [3, 4]. Lymphangiogenesis is modulated by multiple growth factors, of which VEGF-C-VEGFR3 signaling is regarded as the most fundamental and specific pathway. VEGFR3, a membrane receptor tyrosine kinase (RTK), is stimulated by VEGF-C, resulting in activation of AKT and ERK1/2 cascades and enhanced lymphatic endothelial cell growth, migration, tubular formation, and ultimately lymphangiogenesis and lymphatic metastasis [5]. There is abundant preclinical evidence showing that interfering with VEGF-C-VEGFR3 signaling attenuates tumor lymphangiogenesis and metastasis in different animal models [6, 7]. Therefore, targeting the VEGF-C-VEGFR3 pathway constitutes a potential option to treat lymphatic metastasis. SAR131675, a small molecule tyrosine kinase inhibitor, has been found to be highly selective for VEGFR3 to reduce lymphangiogenesis and lymphatic metastasis [8]. However, no Food and Drug Administration (FDA)-approved drugs targeting lymphangiogenesis for the clinical treatment of intractable tumor metastasis exist.

Natural products are abundant in diversity and are a great source of agents for the prevention and treatment of human diseases. Developing lead compounds from natural products is a promising strategy for cancer therapy. Natural stilbenolignans are a class of unconventional lignans formed by the combination of a C6C3 unit with the cinnamoyl moiety of a stilbene and

[1]Key Laboratory of Carcinogenesis and Translational Research (Ministry of Education/Beijing), Department of Biochemistry and Molecular Biology, Peking University Cancer Hospital & Institute, Beijing 100142, China; [2]State Key Laboratory of Natural and Biomimetic Drugs, School of Pharmaceutical Sciences, Peking University, Beijing 100191, China and [3]Key Laboratory of Carcinogenesis and Translational Research (Ministry of Education/Beijing), Department of Laboratory Animal, Peking University Cancer Hospital & Institute, Beijing 100142, China
Correspondence: Chuan-ke Zhao (zhaochk@bjmu.edu.cn) or Li-ke Qu (qulike99@163.com) or Yan-xing Jia (yxjia@bjmu.edu.cn) or Cheng-chao Shou (cshou@vip.sina.com)

Received: 24 January 2022 Accepted: 7 June 2022
Published online: 1 July 2022

are mainly divided into three different families, viz., those isolated from *Arecaceae* (including aiphanol), those isolated from *Fabaceae* (including maackolin), and those isolated from *Gnetaceae* (including lehmbachol D, gnetifolin F and gnetofuran A). However, studies focused on the pharmacological activity of stilbenolignans are lacking. Aiphanol, (chemical name 5-((*E*)-2-((2*S*,3*S*)-3-(4-hydroxy-3,5-dimethoxyphenyl)-2-(hydroxymethyl)-2,3-dihydrobenzo[b][1,4]dioxin-6-yl)vinyl)benzene-1,3-diol), a naturally occurring stilbenolignan, was initially reported to inhibit cyclooxygenase-1 and -2 (COX1/COX2) activity [9]. We recently found that aiphanol exerted an inhibitory effect on angiogenesis by simultaneously suppressing the activity of VEGFR2 and COX2, thereby blocking tumor growth [10]. Interestingly, VEGFR3 was screened as the top-ranked candidate among a subset of aiphanol-targeted kinases [10]. Considering the crucial role of VEGFR3 in lymphangiogenesis, it is valuable to examine whether aiphanol has the potential to inhibit lymphangiogenesis and metastasis by blunting VEGFR3.

Numerous studies have shown positive associations among COX2 activity, the PGE2 level and VEGF-C production in the tumor microenvironment [11, 12]. In addition, recent studies have shown that VEGF-C generated by tumor cells and TAMs directly or indirectly regulates lymphangiogenesis and lymphatic metastasis [13]. Macrophages are the most abundant migratory heterogeneous cell type that respond differentially to various stimulators and thus play distinct roles in cancer progression [14]. It has been postulated that tumor lymphangiogenesis is a complicated process orchestrated by various cell types, and that its functional outcome might be attributed to the interplay of multiple cells and mechanisms [15]. However, whether aiphanol affects the COX2-mediated PGE2-VEGF-C axis in tumor cells and TAMs to regulate lymphangiogenesis and lymphatic metastasis remains unclear.

In the present study, we evaluated the antilymphangiogenic and antimetastatic potency of aiphanol by using in vitro, ex vivo, and in vivo systems. We found that aiphanol directly bound to VEGFR3 and inhibited its kinase activity. In addition, aiphanol blocked the COX2-PGE2-VEGF-C pathway in tumor cells and TAMs to further decrease lymphangiogenesis. Our results opened a new avenue for aiphanol as a potential lead compound to prevent lymphatic dissemination in cancer.

MATERIALS AND METHODS

Tubular formation assay

50 μL growth factor-reduced Matrigel (Corning, NY, USA) was added to each well of a 96-well plate and incubated at 37 °C for 1 h to solidify as the base. Growth factor (100 ng/mL), compounds at different concentrations, or serum-free supernatant from tumor cells and macrophages was mixed with 15,000 LECs to incubate for 10 min, and the mixture was then added to each well for 6 h of incubation. The tubular structure images were acquired under a microscope, and tubular formation was quantified with the Angiogenesis Analyzer plugin in ImageJ.

In vitro spheroid based 3D tubular formation assay

Suspended LECs and a solution of Methocel (1.2% carboxymethylcellulose) were carefully mixed at a ratio of 4:1 (vol/vol), and 25 μL drops (1,000 cells) of the solution were pipetted onto a 10 cm Petri dish using the hanging drop method. The drops were subjected to inverted culture in a humidified incubator for 24 h to form spheroids. A collagen solution (1 mg/mL) and an 80% Methocel solution were mixed in equal volumes, and 200 μL of the mixture was added to each well of a 48-well plate and allowed to polymerize for 30 min as the bottom base. The hanging drops (containing spheroids) were washed off with PBS and spheroids were collected by centrifugation at 170 × *g* for 5 min. The spheroids were resuspended in a Methocel solution containing 20% FBS and mixed with the same volume of collagen. A total of 200 μL of the spheroid-collagen solution was loaded into each well and allowed to polymerize for 30 min as the top matrix. VEGF-C (100 ng/mL) was added with or without aiphanol (30 μM) and incubated for 24 h at 37 °C. SAR131675 (SAR, 30 μM) was used as the positive control. The number of sprouts in the 3D environment was determined by microscopy.

Immunoprecipitation (IP)

An anti-VEGFR3 antibody (2 μg per sample) was added to 500 μL of PBS containing 20 μL of agarose beads and conjugated to the beads by rotating on a shaker for 1 h. HDLECs were homogenized in lysis buffer (100 mM Tris-HCl, pH 7.5, 150 mM NaCl, 20 mM NaF, 1 mM Na_3VO_4, 1 mM EDTA, 1% Triton-X 100 and 1 × protease inhibitor cocktail) and incubated on ice for 30 min. The cell suspension was sonicated and the supernatant was kept after centrifugation at 5000 × *g* for 10 min. Then, 500 μL of cell supernatant was mixed with the anti-VEGFR3 antibody and protein G agarose, and incubated overnight at 4 °C with rotation. The bead complexes were washed 5 times with lysis buffer and eluted with 20 μL of 2 × SDS loading buffer. The samples were subjected to Western blot analysis.

Pull-down assay to evaluate the aiphanol-VEGFR3 interaction

Biotin-labeled aiphanol was first conjugated to 50 μL of Pierce™ avidin-agarose beads (Thermo Fisher Scientific, Madison, USA) in PBS for 2 h. The uncoupled (vehicle) beads and biotin-labeled aiphanol-coupled beads were subsequently mixed with cell lysates in the absence or presence of aiphanol and incubated overnight at 4 °C. The level of captured VEGFR3 was analyzed by Western blot.

Drug affinity responsive target stability (DARTS) assay

HDLECs were homogenized in lysis buffer (100 mM Tris-HCl, pH 7.5, 150 mM NaCl, 20 mM NaF, 1 mM Na_3VO_4, 1 mM EDTA, 1% NP-40 and 0.1% SDS) supplemented with 1 × protease inhibitor cocktail. Lysates were divided into four aliquots (20 μL each) and incubated with aiphanol for 1 h at room temperature. Pronase (2 μg/mL) was added to the indicated aliquots for 15 min in the presence of 10 mM $CaCl_2$ and 0.6% SDS at room temperature. Reactions were terminated by adding 2 × SDS loading buffer and the protein levels were determined by Western blot analysis.

Cellular Thermal Shift Assay (CETSA)

HDLECs were pretreated with DMSO or aiphanol (15 μM) for 2 h and harvested in PBS supplemented with protease inhibitor cocktail. The cells were divided into 7 equal aliquots and heated in a temperature gradient (25 to 63 °C) for 3 min prior to cooling at room temperature. Then, the cells were lysed in buffer (25 mM Tris-HCl, pH 7.5, 5 mM beta-glycerophosphate, 2 mM dithiothreitol, 0.1 mM Na_3VO_4, 10 mM $MgCl_2$) and subjected to four freeze-thaw cycles in liquid nitrogen. Soluble proteins were collected by centrifugation at 5000 × *g* for 15 min at 4 °C, and the supernatants were analyzed by Western blot.

Surface plasmon resonance (SPR) analysis of binding kinetics

Surface plasmon resonance analysis was performed as described previously [10] with slight modifications. Briefly, VEGFR3 was diluted to 20 μg/mL in NaAc (pH 4.0) and immobilized at a flow rate of approximately 10 μL/min for 30 min for the standard amine coupling procedure. Aiphanol was dissolved in DMSO and diluted in buffer containing 10 mM MOPS (pH 7.2), 150 mM NaCl, 1 mM $MgCl_2$ and 0.05% surfactant P20, and the solution was then injected over the functionalized surface at a flow rate of 20 μL/min. Sensorgrams were generated and kinetic parameters were determined with Biacore S200 evaluation software 2.1.

Ex vivo assay of sprouting in lymph nodes
Forty-eight-well plates were coated with 120 μL of Matrigel per well and incubated at 37 °C for 1 h for polymerization. Lymph nodes (LNs) were collected carefully from 7-week-old female BALB/c mice by sterile techiques and sliced into 1 mm thick segments. The node segments were plated on Matrigel surface, 60 μL Matrigel was then added as the top matrix and incubated for 3 h. Then, 500 μL of medium containing 100 ng/mL VEGF-C with or without 30 μM aiphanol/SAR was added to each well. After 1 week, the new lymphatic vessels that sprouted from the nodes were photographed and qualitatively analyzed by immunofluorescence staining.

Matrigel plug assay
Female BALB/c mice (7 weeks old) were randomly grouped ($n = 4$ per group). The mice were given a hypodermic injection of 400 μL of Matrigel containing VEGF-C (500 ng/mL) with or without 30 μM aiphanol/SAR. After 2 weeks, the mice were sacrificed, and the Matrigel plugs were removed and photographed. Liquid nitrogen was used to immediately flash freeze the plugs, and the plugs were then mounted in Tissue-Tek® O.C.T. Compound (Sakura, Torrance, USA) for sectioning with a freezing microtome. Lyve-1 expression in the sections was determined by immunofluorescence staining.

4T1-luc model of lymphatic metastasis
A total of 1×10^6 4T1-luc cells were injected into the mammary fat pad of female BALB/c mice via a minimally invasive surgical procedure. Drugs were delivered by oral administration daily for 2 weeks. Mice were injected intraperitoneally with 150 mg/kg D-luciferin and sacrificed, and the LNs and main organs were harvested to assess luminescence with a Xenogen IVIS-200 system (Caliper LifeSciences, Hopkinton, USA). Living Image software was used to visualize and calculate the luciferin intensity.

Experimental survival studies
Each BALB/c mouse was engrafted with 1×10^6 4T1-luc cells in a mammary fat pad via a minimally invasive surgical procedure. The mice were randomly grouped and treated with aiphanol or SAR by oral administration daily for 3 weeks. The survival time of each mouse was recorded, and the Kaplan-Meier survival curve was plotted.

Ethics statement
BALB/c mice were purchased from HFK BIOSCIENCE CO.,LTD (Beijing, China) and maintained in a specific pathogen-free environment at the Department of Laboratory Animal of Peking University Cancer Hospital & Institute. Animal experiments was approved by the Ethics Committee of Peking University Cancer Hospital & Institute (license number: Animal-2012-01). All experimental procedures involving mice were performed in accordance with the guidelines of the animal welfare institution (NIH #85-23).

Statistical analysis
GraphPad Prism 8.0 software was utilized to perform two-tailed student's *t* test and one-way ANOVA. Kaplan-Meier analysis was performed to evaluate the survival times of tumor-bearing mice. Values are shown as the mean ± standard errors of the mean (SEM). *P* value of less than 0.05 was considered statistically significant. $^*P < 0.05$; $^{**}P < 0.01$; $^{***}P < 0.001$; n.s., not significant.

RESULTS

VEGFR3 is a direct target of aiphanol
Considering that aiphanol (Fig. 1a) strongly interfered with VEGFR3 activity in the screening test [10], we further carried out an in vitro ADP-Glo™ assay using recombinant human VEGFR3 and found that aiphanol inhibited VEGFR3 kinase activity with an IC_{50} value of 0.29 μM (Fig. 1b). Since VEGFR3 is expressed predominantly in the adult lymphatic endothelium [16], we then chose human dermal lymphatic endothelial cells (HDLECs) to investigate the effects of aiphanol on endogenous VEGFR3. The uptake of FAM-coupled aiphanol by HDLECs was verified by flow cytometry (Supplementary Fig. S1a). FAM-aiphanol entered HDLECs and costained with the membrane dye DiI (Supplementary Fig. S1b). Moreover, VEGF-C-stimulated tyrosine phosphorylation of VEGFR3 was diminished by aiphanol, as determined by immunoprecipitation with VEGFR3 antibody followed by Western blot analysis with a phosphotyrosine antibody (Fig. 1c, d). Through immunofluorescence staining with a phosphosite-specific antibody, we confirmed that aiphanol blocked VEGFR3-Tyr^{1230} phosphorylation (Fig. 1e). Additionally, we found that aiphanol suppressed the phosphorylation of kinases downstream of VEGFR3, including FAK, AKT, and ERK1/2 (Fig. 1d). The inhibitory effect of aiphanol on these kinases was stronger than that of SAR131675 (SAR), a selective inhibitor of VEGFR3 (Fig. 1d). These results indicate the capacity of aiphanol to antagonize VEGFR3 activity in vitro.

To explore the possible interaction mode between aiphanol and VEGFR3, structural dynamics simulation was utilized to show that aiphanol binds to the catalytic domain of VEGFR3 (binding energy = −10.86 kcal/mol). Aiphanol might occupy the ATP-binding domain of VEGFR3 and block its ATP-mediated phosphorylation. Specifically, aiphanol was mainly located in the hydrophobic cavity of VEGFR3, which was composed of Leu851, Ala877, Lys879, Glu896, Leu900, Val925, Val927, Glu928, Phe929, Cys930, Lys931, Tyr932, Asn934, Asn937, Leu1044, Asp1055 and Phe1056. The hydroxyl groups on the benzene rings of aiphanol formed three hydrogen bonds, one each with Asn934, Asn937 and Asp1055. Additionally, two hydrogen-bonding interactions were found to occur between the hydroxyl group on the benzo-1, 4-dioxane moiety and Cys930, and Lys931. Two benzene rings and the benzo-1, 4-dioxane moiety shared strong hydrophobic contacts with hydrophobic amino acids surrounding the pocket (Leu851, Ala877, Lys879, Glu896, Leu900, Val925, Val927, Glu928, Phe929, Tyr932, Leu1044 and Phe1056), further enhancing the affinity of aiphanol for VEGFR3 (Fig. 1f, g). Alignment of the intracellular domains in VEGFR3 and VEGFR2 revealed that the aiphanol-binding residues of these two kinases were largely conserved, with few differences (Supplementary Fig. S1c), possibly partially explaining why the inhibitory effect of aiphanol on VEGFR3 (97%) was stronger than that on VEGFR2 (85%) [10]. To support this prediction, we investigated whether aiphanol can bind to the VEGFR3 protein and promote its stability with two target binding approaches. Small molecule inhibitors can form a ligand-protein complexes with the target protein to hamper protein function and maintain protein stability [17]. The result of the drug affinity responsive target stability (DARTS) assay revealed that aiphanol dose-dependently inhibited pronase-induced degradation of VEGFR3, enabling VEGFR3 to resist proteolysis (Fig. 1h). In the cellular thermal shift assay (CETSA) [18], we found that aiphanol efficiently prevented VEGFR3 protein degradation in a temperature-dependent manner (Fig. 1i). Double immunofluorescence staining showed partial colocalization of FAM-labeled aiphanol and the VEGFR3 protein in HDLECs (Supplementary Fig. S1d). Furthermore, biotin-labeled aiphanol effectively captured VEGFR3 from HDLECs lysates, while the level of precipitated VEGFR3 was obviously perturbed in the presence of extra unlabeled aiphanol as a competitor (Fig. 1j). Moreover, surface plasmon resonance (SPR) analysis confirmed the direct binding of aiphanol and VEGFR3 with an equilibrium dissociation constant (KD) of 0.48 μM (Fig. 1k). However, aiphanol did not interfere with the VEGF-C-VEGFR3 interaction, as determined by biolayer interferometry (BLI) (Fig. 1l). Collectively, these results demonstrated VEGFR3 as a direct cellular target of aiphanol. Trafficking of VEGFR3 is critical for the control of its function as an RTK [6]. The membrane localization of VEGFR3 was diminished by VEGF-C

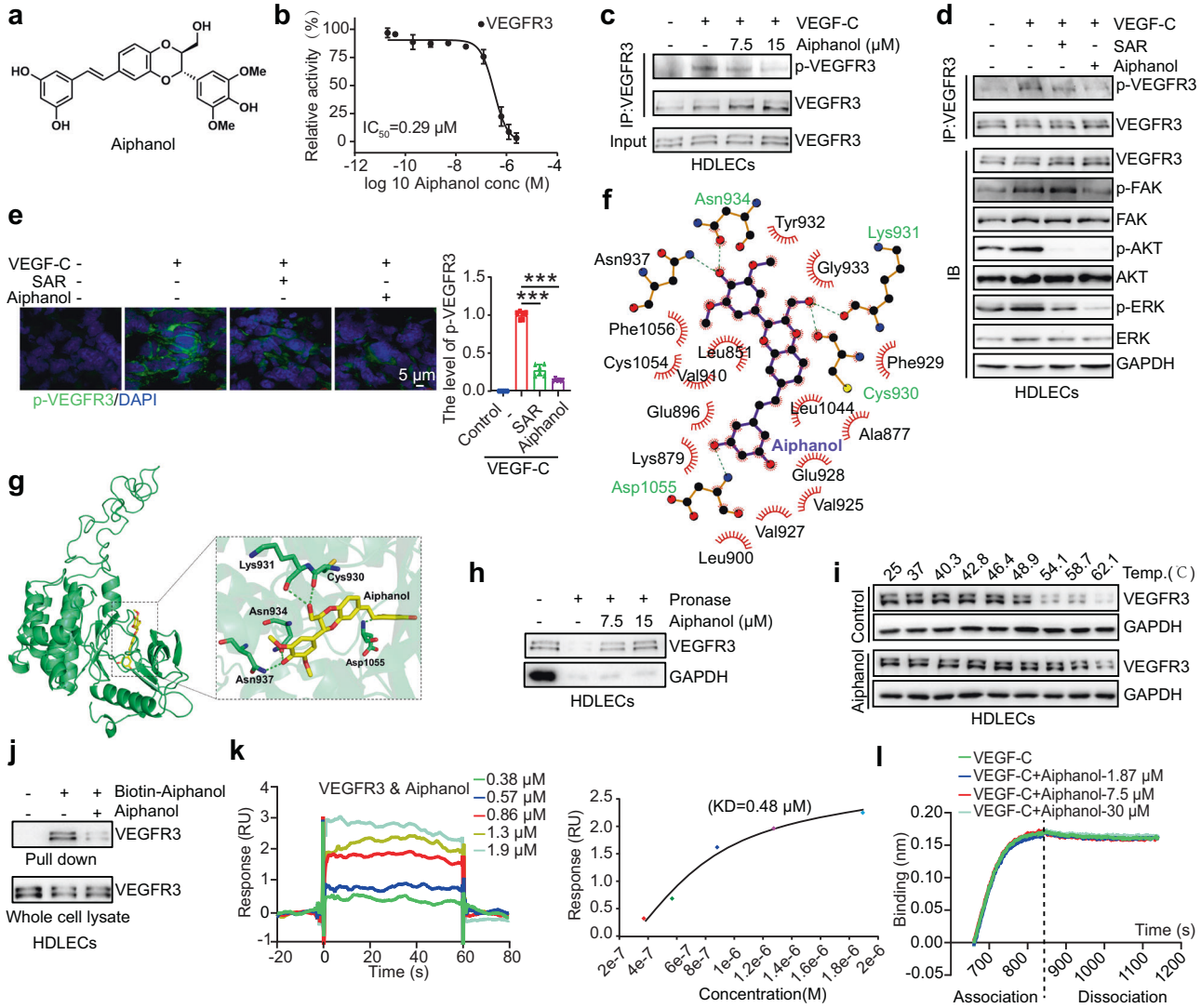

Fig. 1 VEGFR3 is a direct target of aiphanol. a Structure of aiphanol. **b** Dose-response curves for recombinant human VEGFR3 and aiphanol in the ADP-Glo™ kinase assay measuring autophosphorylation of the VEGFR3 kinase domain in vitro. VEGFR3 was incubated with aiphanol at concentrations as indicated in the presence of ATP and the kinase detection substrate poly (Glu:Tyr 4:1). **c** HDLECs were pretreated with the indicated concentrations of aiphanol for 1 h prior to VEGF-C (100 ng/mL) stimulation for 15 min. Lysates were analyzed by immunoprecipitation and Western blot. **d** HDLECs were pretreated with 15 μM aiphanol or SAR131675 (SAR; as the positive control) for 1 h prior to VEGF-C (100 ng/mL) treatment for 15 min. Lysates were subjected to immunoprecipitation and Western blot with the indicated antibodies. **e** Immunofluorescence staining of p-VEGFR3-Tyr^{1230} (green) in HDLECs ($n = 6$ per group). Scale bar, 5 μm. **f**, **g** Prediction of the aiphanol-VEGFR3 docking mode. The dotted green lines indicate hydrogen bonds and red gear shapes indicate hydrophobic interactions. 2D representation (**f**) and 3D representation (**g**) of aiphanol docking in the VEGFR3 binding sites were shown. **h** DARTS assay. HDLECs lysates were incubated with pronase (2 μg/mL) after treatment with the indicated concentrations of aiphanol for 1 h, and the level of VEGFR3 was determined by Western blot. **i** HDLECs were exposed to aiphanol (15 μM) or vehicle for 2 h prior to the cellular thermal shift assay (CETSA). **j** Avidin-agarose pull-down of biotin-labeled aiphanol and VEGFR3 from HDLECs lysates with or without an excess of unlabeled aiphanol. The level of VEGFR3 was measured by Western blot. **k** Sensorgram showing the binding of aiphanol to VEGFR3 (left) and the steady-state KD values at equilibrium fitted using Biacore software (right). **l** BLI analysis of the VEGF-C-VEGFR3 interaction. The association and dissociation curves of VEGF-C-VEGFR3 binding in the absence or presence of the indicated concentrations of aiphanol were shown. The data were represented as the mean ± SEM. ***$P < 0.001$.

stimulation (Supplementary Fig. S2a, b), which was consistent with the results of a previous study [6]. However, aiphanol had no such effect. In addition, aiphanol did not affect VEGF-C-induced dissociation of VEGFR3 from the membrane (Supplementary Fig S2a, b). By costaining of the early endosome marker EEA1, we found that aiphanol had no significant influence on VEGF-C-induced endocytosis of VEGFR3 (Supplementary Fig. S2a). By costaining VEGFR3 with Giantin, a Golgi membrane protein, we found that aiphanol did not increase or decrease the Golgi pool of VEGFR3 (Supplementary Fig. S2b).

Aiphanol inhibits lymphangiogenesis

Consistent with the role of the VEGF-C-VEGFR3 axis as a key driver of lymphangiogenesis [6, 7], VEGF-C promoted HDLECs to form tube-like structures on the matrix, however, the enhancement was minimal in response to EGF or bFGF (Fig. 2a). Aiphanol suppressed both basal and growth factor-stimulated lymphatic vessel formation (Fig. 2a), and this effect was dose-dependent (Fig. 2b). The HDLECs spheroids sprouting assay mimics the 3D culture environment in which cells can grow, migrate, and generate new buds. The number of newly formed spheroid branches

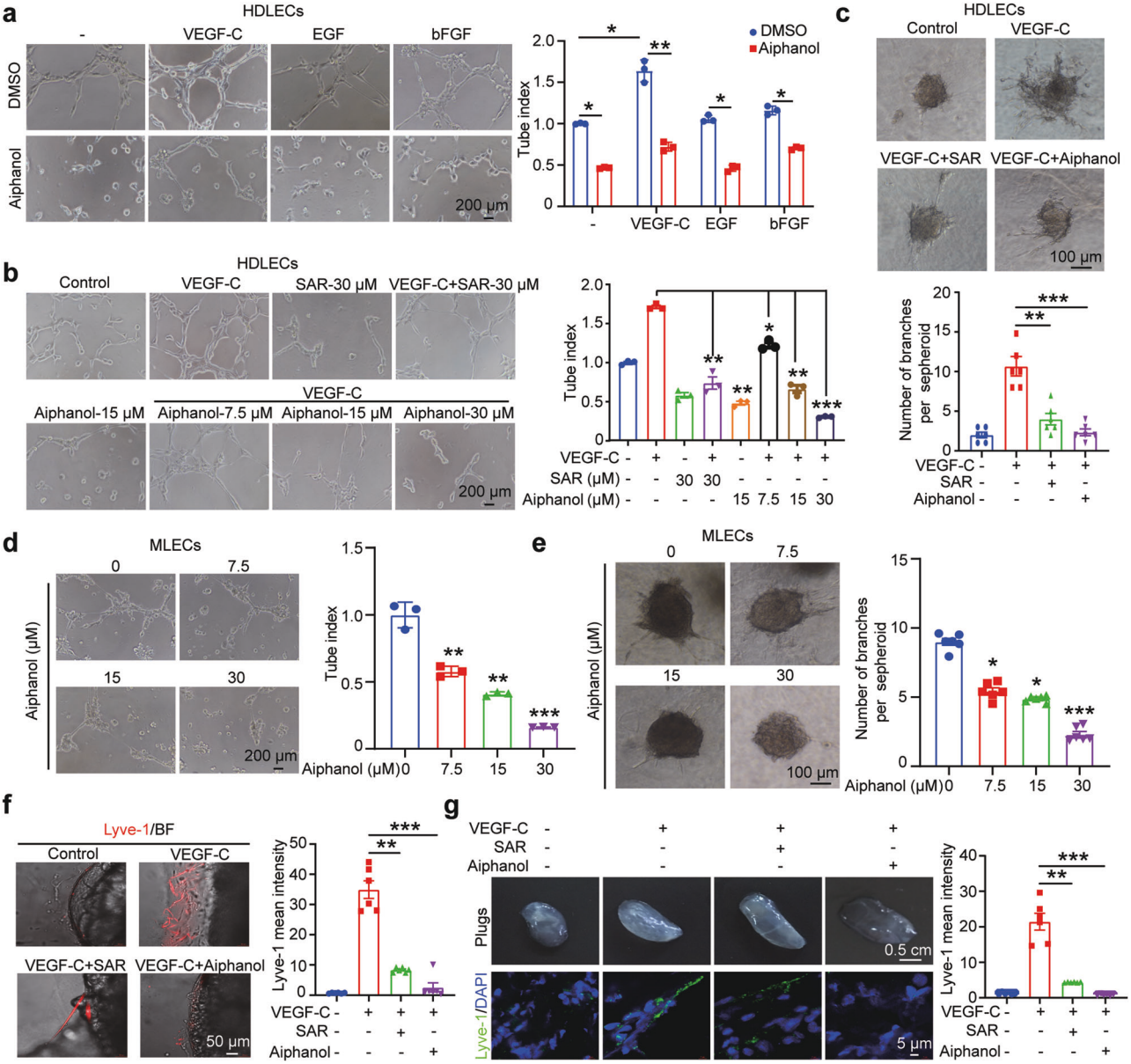

Fig. 2 Aiphanol inhibits lymphangiogenesis. a Effects of aiphanol (30 μM) on VEGF-C-, EGF- or bFGF (all at 100 ng/mL)-driven tubular formation of HDLECs. The tube index was quantified by ImageJ ($n = 3$ per group). Scale bar, 200 μm. **b** Effects of the indicated concentrations of aiphanol or SAR on VEGF-C (100 ng/mL)-induced tubular formation of HDLECs. Tubular structures were imaged and the tube index was determined ($n = 3$ per group). Scale bar, 200 μm. **c** Sprouting from HDLECs spheroids immersed in a collagen-Methocel mixture after exposure to 30 μM aiphanol or SAR in combination with VEGF-C (100 ng/mL) for 24 h ($n = 6$ per group). Scale bar, 100 μm. **d** Effects of the indicated concentrations of aiphanol on the tubular formation of MLECs ($n = 3$ per group). Scale bar, 200 μm. **e** Effects of the indicated concentrations of aiphanol on spheroids sprouting of MLECs ($n = 6$ per group). Scale bar, 100 μm. **f** Effects of aiphanol (30 μM) on VEGF-C (100 ng/mL)-induced sprouting in axillary LN segments (~1 mm^3) from BALB/c mice. Lymphatic vessel structures sprouting from LNs were stained with anti-Lyve-1 antibody (red) ($n = 6$ per group). Scale bar, 50 μm. **g** A Matrigel plug assay was performed to evaluate the suppressive effect of aiphanol on the formation of newly lymphatic vessels in vivo ($n = 4$ per group). Frozen sections of Matrigel plugs were probed with anti-Lyve-1 antibody (green). Scale bar, 0.5 cm (plugs) and 5 μm (sections). The data were shown as the mean ± SEM. * $P < 0.05$; ** $P < 0.01$; *** $P < 0.001$.

stimulated by VEGF-C was evidently decreased by aiphanol (Fig. 2c). Similarly, aiphanol decreased the lymphatic vessel formation and spheroid sprouting of mouse lymphatic endothelial cells (MLECs) in a dose-dependent manner (Fig. 2d, e). Sprouting in axillary LNs isolated from mice was also blocked by aiphanol, as validated by immunofluorescence staining of the lymphatic vessel marker Lyve-1 (Fig. 2f). Furthermore, we found that the density of Lyve-1 was decreased upon aiphanol treatment in the Matrigel plug assay (Fig. 2g), indicating that aiphanol inhibits lymphatic vasculature formation in vivo.

Aiphanol suppresses cell proliferation, motility and lymphangiogenesis in a VEGFR3-dependent fashion

Aiphanol did not affect the proliferation of MLECs (Fig. 3a), but the proliferation of HDLECs was inhibited by aiphanol in a time- and concentration-dependent manner (Fig. 3b), suggesting a cell-type specific effect on proliferation. Aiphanol increased the proportion of G1- phase cells in HDLECs (Fig. 3c), but it did not induce apoptosis between 24 h and 96 h (Supplementary Fig. S3a, b). Interestingly, aiphanol transiently induced autophagic flux in HDLECs, as indicated by the increased expression of LC3-II and Beclin 1

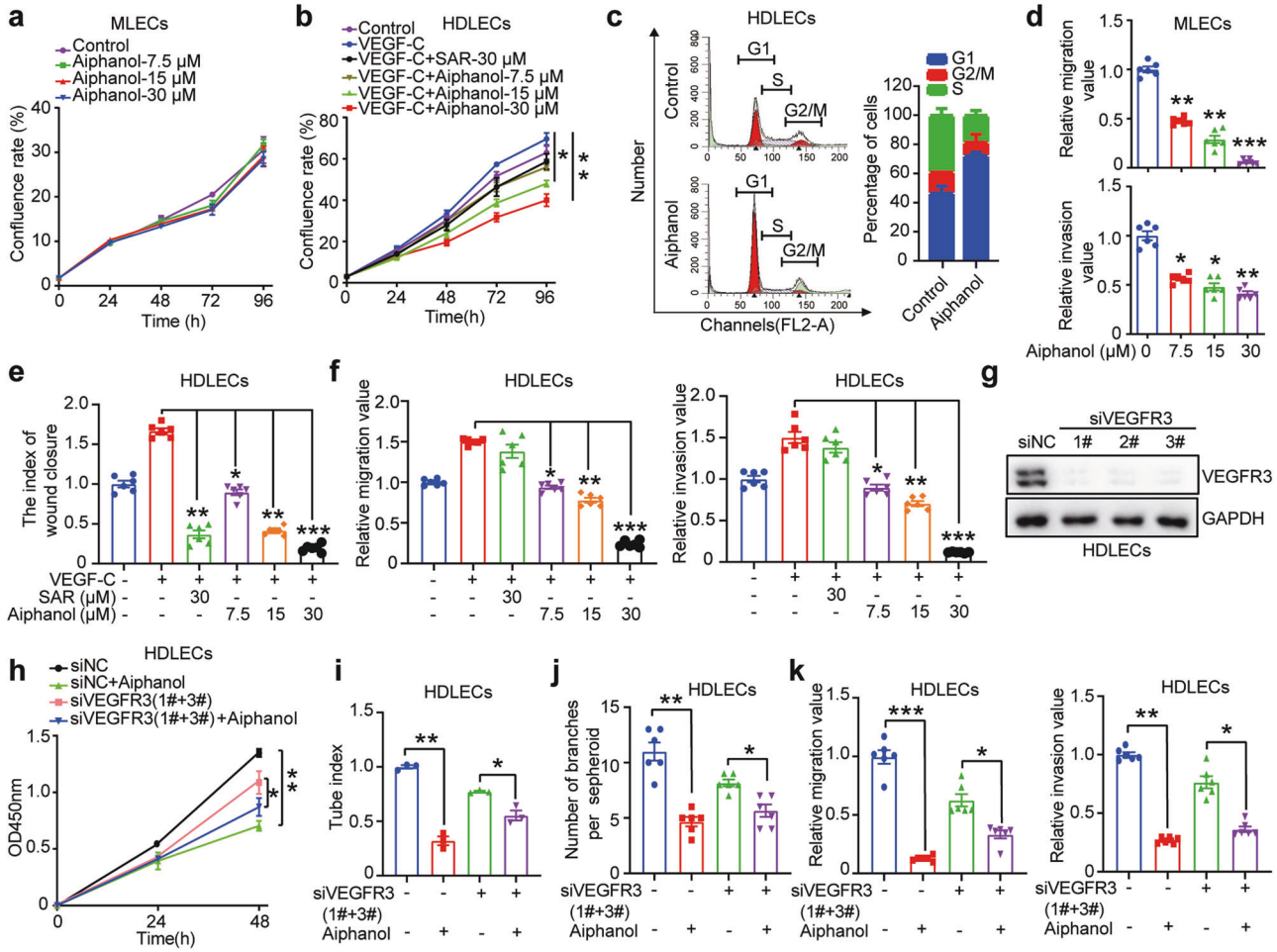

Fig. 3 VEGFR3 contributes to the effects of aiphanol on LECs. a MLECs were treated with the indicated concentrations of aiphanol, and cell proliferation was monitored every 24 h with a CloneSelect Imager ($n = 3$ per group). **b** HDLECs were exposed to indicated concentrations of aiphanol and SAR in addition to 100 ng/mL VEGF-C, and cell proliferation was quantified at 24 h intervals with a CloneSelect Imager ($n = 3$ per group). **c** The cell-cycle distribution of HDLECs following exposure to 30 μM aiphanol or vehicle control for 24 h was determined by flow cytometry. **d** Transwell assays were performed to evaluate the effects of aiphanol on the migration and invasion of MLECs ($n = 6$ per group). **e** A wound healing assay was used to assess the effects of aiphanol and SAR on VEGF-C (100 ng/mL)- stimulated migration of HDLECs ($n = 6$ per group). **f** Transwell assays were performed to evaluate the effects of aiphanol and SAR on VEGF-C (100 ng/mL)-stimulated migration and invasion of HDLECs ($n = 6$ per group). **g** Western blot analysis of VEGFR3 expression in HDLECs transfected with VEGFR3 siRNA or scrambled siRNA for 48 h. **h** Impacts of VEGFR3 depletion on aiphanol-induced inhibition of HDLECs proliferation. Cells were treated with or without 30 μM aiphanol for 24-48 h after transfection with VEGFR3 siRNA or scrambled siRNA for 48 h ($n = 3$ per group). **i** Tubular formation analysis of HDLECs treated with or without 30 μM aiphanol for 6 h following transfection with VEGFR3 siRNA or scrambled siRNA for 48 h ($n = 3$ per group). **j** Analysis of HDLECs spheroids sprouting in the absence or presence of 30 μM aiphanol for 24 h after transfection with VEGFR3 siRNA or scrambled siRNA for 48 h ($n = 6$ per group). **k** Impacts of VEGFR3 silencing on aiphanol-induced inhibition of HDLECs motility. Cells were transfected with VEGFR3 siRNA or scrambled siRNA for 48 h prior to Transwell migration and invasion assays over a 24 h time course in the absence or presence of 30 μM aiphanol ($n = 6$ per group). The data were represented as the mean ± SEM. $^*P < 0.05$; $^{**}P < 0.01$; $^{***}P < 0.001$.

(Supplementary Fig. S3b) accompanied by enhanced autophagosome formation (Supplementary Fig. S3c). Through senescence-associated β-galactosidase staining, we found that the effect of aiphanol on senescence induction was statistically insignificant (Supplementary Fig. S3d). Therefore, aiphanol-induced proliferation inhibition was correlated with cell-cycle arrest and autophagy in HDLECs. Next, we found that aiphanol reduced the motility of MLECs in the Transwell migration and invasion assays (Fig. 3d). Likewise, aiphanol's inhibitory effects on wound healing, migration, and invasion were observed in HDLECs (Fig. 3e, f). Importantly, following VEGFR3 knockdown in HDLECs (Fig. 3g), the inhibitory effects of aiphanol on cell proliferation (Fig. 3h, Supplementary Fig. S4a), tube formation (Fig. 3i, Supplementary Fig. S4b), spheroid sprouting (Fig. 3j) and motility (Fig. 3k) were attenuated. These results further substantiated VEGFR3 as a critical target mediating the inhibitory effect of aiphanol on lymphangiogenesis.

Aiphanol decreases lymphatic metastasis and improves survival in a 4T1-luc murine breast cancer model

To further evaluate the effect of aiphanol on lymphatic metastasis in vivo, we utilized 4T1-luc murine breast adenocarcinoma cells, which have a high rate of lymphatic dissemination [19]. We injected 4T1-luc cells into the mammary fat pads of BALB/c mice via a minimally invasive surgical procedure and orally administered aiphanol to the mice. We observed that the bioluminescence intensities in the forelimbs, hindlimbs, axillary LNs and inguinal LNs were dramatically reduced upon aiphanol treatment (Fig. 4a). Aiphanol also inhibited distant metastasis of 4T1-luc cells to the spleen and kidney (Fig. 4a). These results strongly validated the antilymphatic metastasis effect of aiphanol in vivo. Immunofluorescence staining of frozen sections of primary tumors revealed decreased levels of Lyve-1 and p-VEGFR3 after aiphanol treatment (Fig. 4b), further confirming aiphanol's ability to inhibit

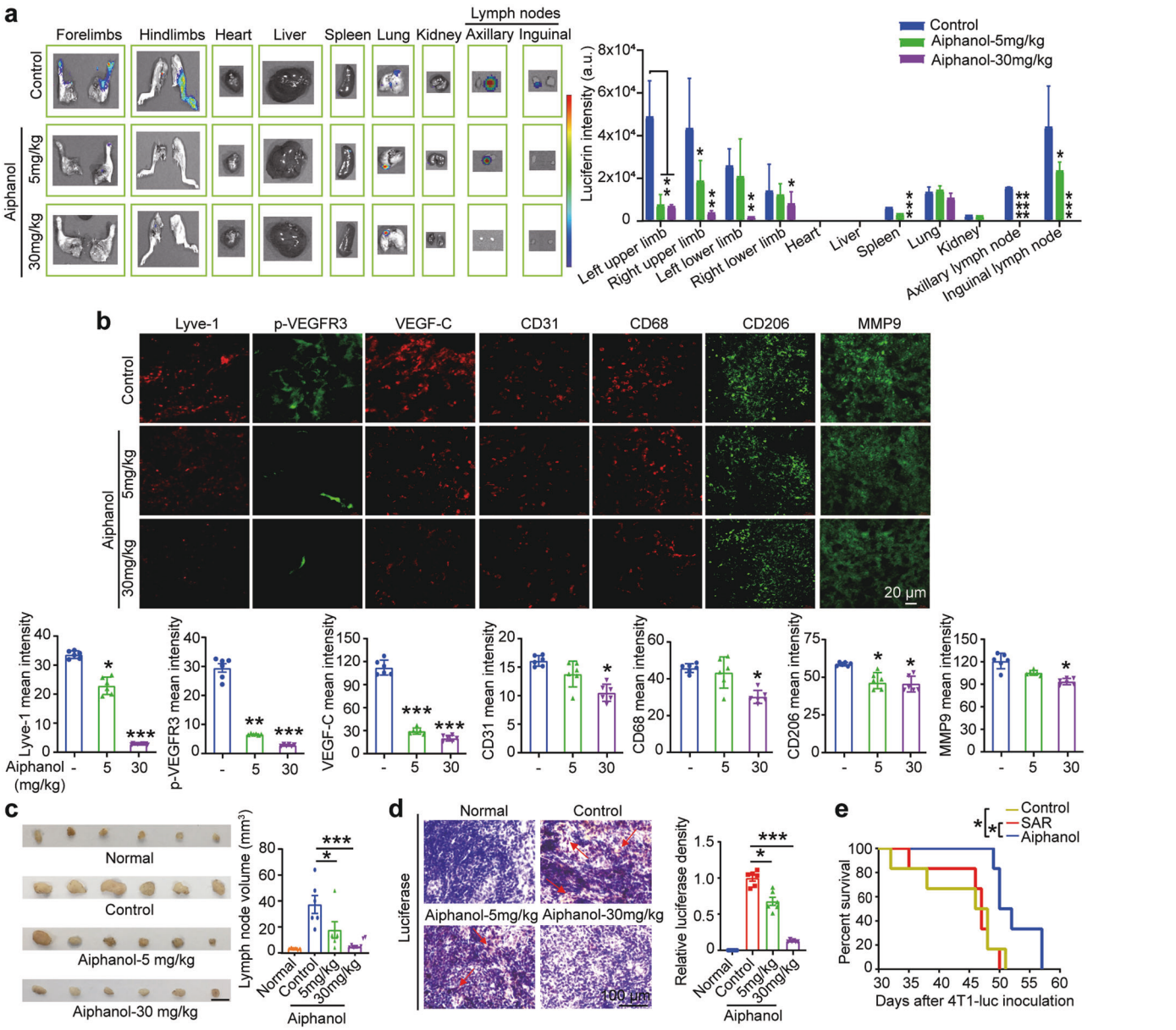

Fig. 4 Aiphanol decreases lymphatic metastasis and improves survival in a murine 4T1-luc breast cancer model. a Left, representative pictures of bioluminescence signals in main organs and LNs from mice. Right, quantification of the bioluminescence intensity (indicating the presence of invasive 4T1-luc cells) in tissues ($n = 3$ per group). **b** Frozen sections from primary 4T1-luc tumors were immunostained with the indicated antibodies. Upper, representative images; lower, quantitative analysis ($n = 6$ per group). Scale bar, 20 μm. **c** Left, images of axillary LNs from mice with different treatments were shown (scale bar, 5 mm). Right, the volume of axillary LNs was quantified ($n = 6$ per group). **d** IHC staining of luciferase expression (brown areas, indicated by red arrows) in axillary LNs from mice. **e** Kaplan-Meier survival curves showing the efficacy of aiphanol or SAR (both 30 mg/kg) in BALB/c mice bearing 4T1-luc breast carcinomas ($n = 6$ per group). The data were shown as the mean ± SEM. *$P < 0.05$; **$P < 0.01$; ***$P < 0.001$.

VEGFR3 phosphorylation and lymphangiogenesis. The level of the microvascular marker CD31 was also decreased by aiphanol, which was consistent with our recent findings [10]. In addition, the volume of axillary LNs was greatly decreased by aiphanol (Fig. 4c). A reduction in the number of luciferase-positive 4T1-luc cells within axillary LNs was observed in the aiphanol-treated group (Fig. 4d), suggesting that aiphanol blocked cancer cell invasion or intravasation into axillary LNs through lymphatic vessels. Next, we established the survival curves for the 4T1-luc tumor model. The mean survival times in the vehicle control, aiphanol and SAR groups were 43.8, 52.5 and 45.5 d, respectively. The aiphanol treatment group showed an extended survival time compared to those in the vehicle control ($P = 0.016$) and SAR treatment groups ($P = 0.0149$) (Fig. 4e). Therefore, the inhibitory effect of aiphanol on lymphatic metastasis is associated with a prolonged lifespan in 4T1 tumor-bearing mice.

Aiphanol inhibits cancer cell invasiveness and paracrine-stimulated lymphangiogenesis by targeting COX2

Evaluation of primary 4T1-luc tumor sections revealed that aiphanol decreased MMP-9 expression (Fig. 4b), suggesting that aiphanol may counteract the extravasation of 4T1 cells, another critical step of lymphatic metastasis. Aiphanol slightly decreased proliferation of 4T1-luc cells (Fig. 5a). Aiphanol did not affect migration (Fig. 5b), but dose-dependently decreased the invasion of 4T1-luc cells (Fig. 5c). Because the expression of MMP2/9 is

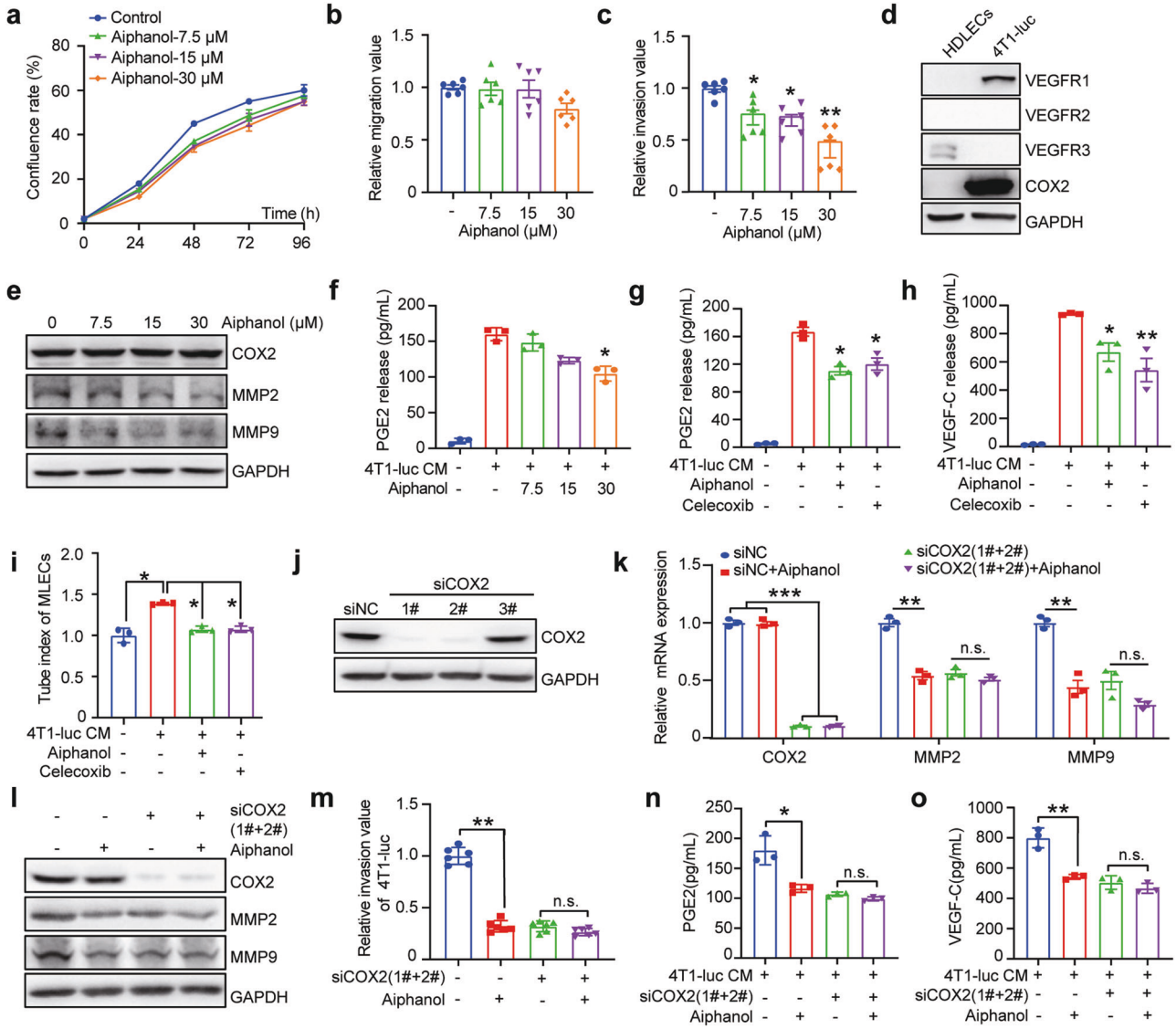

Fig. 5 Aiphanol inhibits cancer cell invasiveness and paracrine-stimulated lymphangiogenesis by targeting COX2. a Effect of aiphanol on 4T1-luc cell proliferation. **b**, **c** Effects of aiphanol on the Transwell migratory (**b**) and invasive (**c**) abilities of 4T1-luc cells ($n = 6$ per group). **d** Levels of the indicated proteins in HDLECs and 4T1-luc cells. **e** Western blot analysis of COX2, MMP-2 and MMP-9 expression in 4T1-luc cells treated with the indicated concentrations of aiphanol for 24 h. **f** ELISA analysis of PGE2 in 4T1-luc cells treated with the indicated concentrations of aiphanol for 24 h. **g**, **h** 4T1-luc cells were treated with 30 μM aiphanol or celecoxib (as the positive control) for 24 h, and the concentrations of PGE2 (**g**) and VEGF-C (**h**) in the CM were then measured by ELISA ($n = 3$ per group). **i** 4T1-luc cells were treated with 30 μM aiphanol or celecoxib for 24 h, and then cultured in serum-free medium for another 24 h. CM was harvested for a tubular formation assay in MLECs ($n = 3$ per group). **j** Western blot analysis of COX2 expression in 4T1-luc cells transfected with COX2 siRNA or scrambled siRNA. Effects of COX2 silencing and aiphanol treatment on the transcript (**k**) and protein (**l**) levels of MMP-2 and MMP-9 were analyzed. **m** Effects of COX2 depletion and aiphanol treatment on 4T1-luc cell invasion. Cells were transfected with COX2 siRNA or scrambled siRNA for 48 h prior to invasion assay in the absence or presence of 30 μM aiphanol for 24 h ($n = 6$ per group). ELISA analysis was performed to detect PGE2 (**n**) and VEGF-C (**o**) expression in the CM from 4T1-luc cells treated with 30 μM aiphanol after COX2 silencing ($n = 3$ per group). The data were shown as the mean ± SEM. $^*P < 0.05$; $^{**}P < 0.01$; $^{***}P < 0.001$; n.s., not significant.

partially controlled by the COX2-PGE2 pathway [20], and aiphanol could function as a direct inhibitor of COX2's enzymatic activity [10], we then sought to examine the contribution of COX2 to aiphanol-regulated MMP2/9 expression. 4T1-luc cells were shown to have abundant COX2 protein expression but deficient VEGFR3 expression (Fig. 5d). Aiphanol decreased the protein levels of MMP-2 and MMP-9, but did not affect that of COX2 (Fig. 5e). However, the PGE2 level in the conditioned medium (CM) from 4T1-luc cells was decreased (Fig. 5f, g), suggesting that COX2 activity was inhibited by aiphanol. Secretion of VEGF-C, another downstream factor of PGE2, was decreased by aiphanol (Fig. 5h), consistent with the in vivo observation (Fig. 4b). CM from 4T1-luc cells promoted tubular formation of MLECs, whereas CM from aiphanol-treated 4T1-luc cells had no such effect (Fig. 5i). After siRNA-mediated silencing of COX2 (Fig. 5j), aiphanol's inhibitory effects on MMP-2 and MMP-9 expression (Fig. 5k, l) and cell invasion (Fig. 5m) were greatly diminished. COX2 silencing limited the secretion of PGE2 and VEGF-C and ameliorated the inhibitory effect of aiphanol on the release of both two factors (Fig. 5n, o, Supplementary Fig. S5a, b). These results collectively suggest that targeting the COX2-PGE2-MMP2/9 and COX2-PGE2-VEGF-C axes in cancer cells with aiphanol may inhibit cancer cell invasiveness and paracrine-stimulated lymphatic vessel formation, respectively.

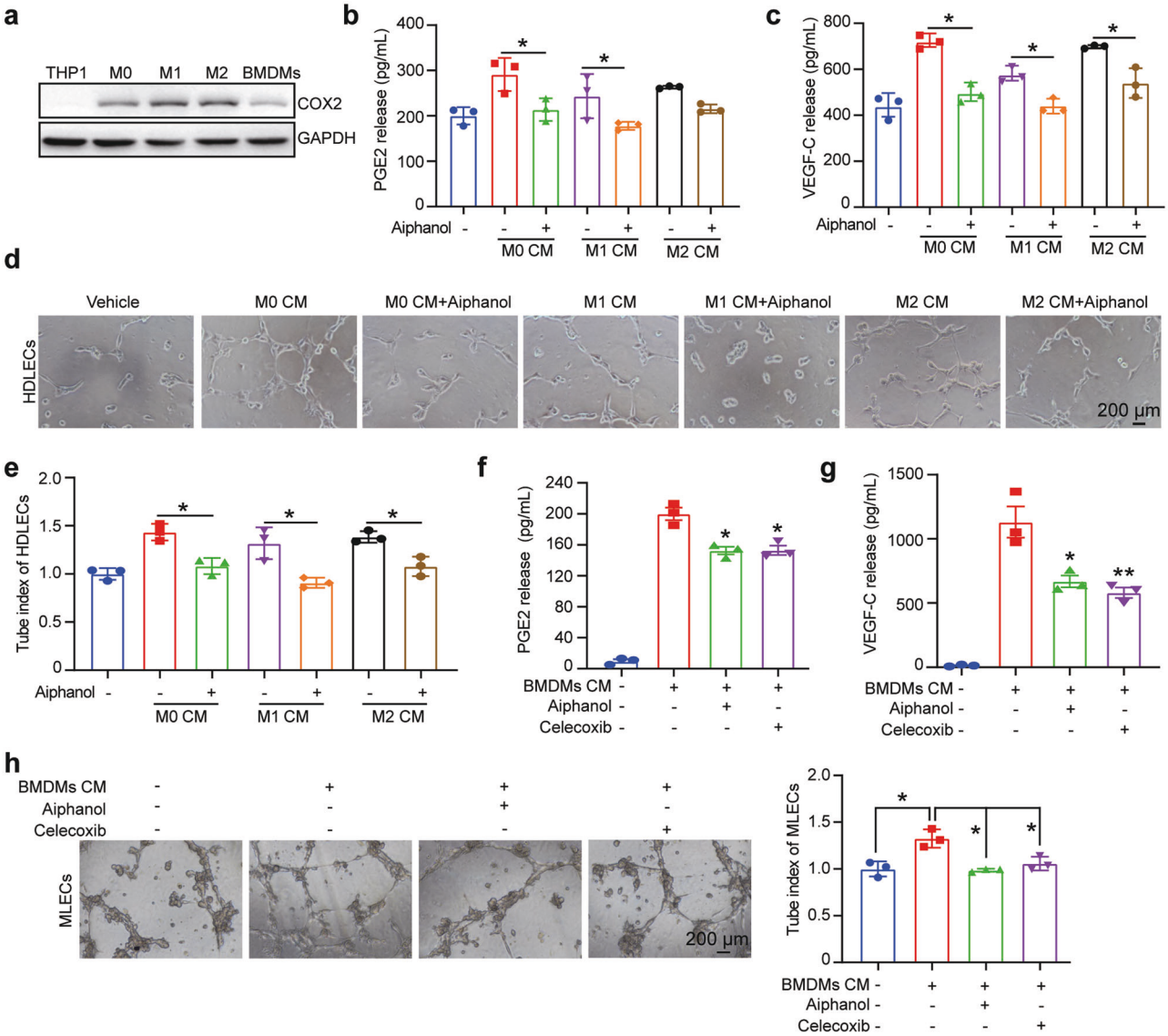

Fig. 6 Aiphanol inhibits TAM infiltration and TAM-promoted lymphangiogenesis by targeting COX2. a COX2 expression in THP-1 cell, THP-1-derived macrophages and BMDMs. **b**, **c** Effect of aiphanol (30 μM) treatment for 24 h on the levels of PGE2 (**b**) and VEGF-C (**c**) in the CM from THP-1-derived macrophages ($n = 3$ per group). **d**, **e** Representative photographs showing the effects of CM from THP-1-derived macrophages treated with aiphanol (30 μM) on tubular formation of HDLECs ($n = 3$ per group), Scale bar, 100 μm, (**d**). The total length of the tubular network was quantified (**e**). Effects of aiphanol or celecoxib (both at 30 μM) treatment for 24 h on the concentrations of PGE2 (**f**) and VEGF-C (**g**) in the CM from BMDMs ($n = 3$ per group). **h** Effects of CM from aiphanol or celecoxib (both at 30 μM)- treated BMDMs on the tubular formation in MLECs ($n = 3$ per group). The data were represented as the mean ± SEM. $^*P < 0.05$; $^{**}P < 0.01$.

Aiphanol inhibits TAM infiltration and TAM-promoted lymphangiogenesis by targeting COX2

Aiphanol's inhibitory effects on the secretion of PGE2 and VEGF-C as well as the expression of MMP2/9 emphasize that this agent has a potent capacity to modulate the tumor microenvironment. TAMs are one of the major cellular components of the tumor microenvironment, and their recruitment and polarization are regulated by the COX2-PGE2 axis. Moreover, TAMs per se can secret PGE2 and VEGF-C as well as a plethora of cytokines, chemokines, and proteases to enhance tumor progression [21]. By immunofluorescent staining of primary 4T1-luc tumor sections, we found that the densities of both CD68 positive (a pan-macrophage marker) and CD206 positive (a M2 macrophage marker) TAMs were decreased by aiphanol (Fig. 4b), implying that aiphanol could inhibit TAM infiltration. To validate the above in vivo observation, we utilized THP-1 human leukemia monocytic cell derived M0, M1, and M2 subsets of macrophages, which expressed COX2 upon differentiation (Fig. 6a). We found that aiphanol decreased the levels of PGE2 and VEGF-C in the CM from all these subsets (Fig. 6b, c). Consistent with this finding, CM from aiphanol-treated cells of these subsets had diminished capacity to stimulate tubular formation of HDLECs (Fig. 6d, e). We further used murine bone marrow-derived macrophages (BMDMs), which also expressed COX2 (Fig. 6a). CM from aiphanol-treated BMDMs had decreased amounts of PGE2 and VEGF-C (Fig. 6f, g), and exhibited an attenuated potential to stimulate tube formation of MLECs (Fig. 6h). Thus, the inhibition of COX2-PGE2-VEGF-C axis in TAMs induced by aiphanol may also contribute to its ability to counteract tumor lymphangiogenesis.

DISCUSSION

Tumor-associated lymphatic vessels are closely correlated with metastasis and clinical outcomes in various types of cancer

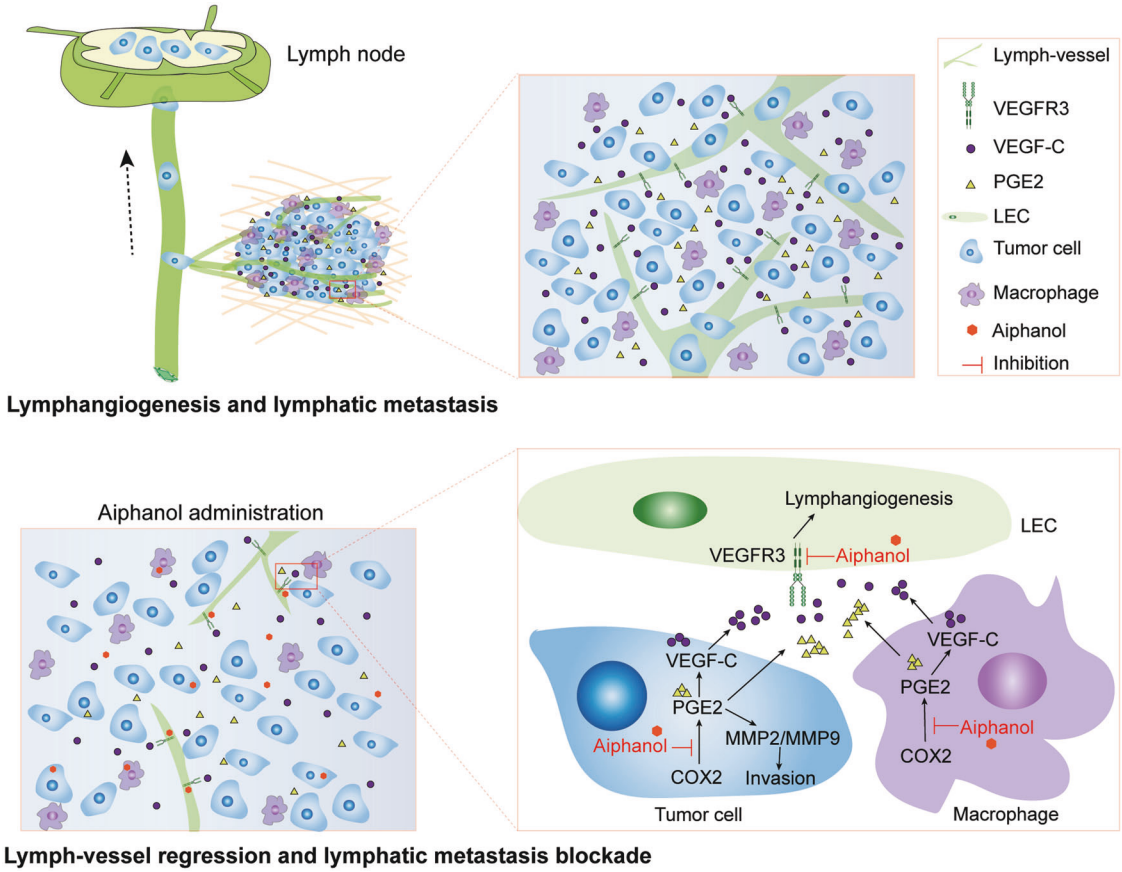

Fig. 7 The schematic model of aiphanol's effects on lymphangiogenesis and lymphatic metastasis. Aiphanol prevents lymphangiogenesis and lymphatic metastasis by orchestrating interactions among multiple molecules and multiple cell types in the tumor microenvironment.

[22–24]. Herein, the antilymphangiogenic and antilymphatic metastatic functions of aiphanol were explored. We showed that aiphanol inhibits VEGFR3 kinase activity through direct binding. Aiphanol downregulates the COX2-PGE2-VEGF-C and COX2-PGE2-MMP2/9 axes in tumor cells and the COX2-PGE2-VEGF-C axis in macrophages, thereby reducing TAM infiltration to collaboratively suppress lymphangiogenesis, lymphatic metastasis and extend the survival of tumor-bearing mice (Fig. 7).

We found that aiphanol inhibited the phosphorylation of VEGFR3-Tyr^{1230}. VEGFR3-Tyr^{1230} is in the cytoplasmic carboxyl-terminal tail of VEGFR3 and is an important regulatory tyrosine phosphorylation site with potential signal transduction capacity [25]. VEGFR3-Tyr^{1230} and VEGFR3-Tyr^{1231} contribute together with VEGFR3-Tyr^{1337} to endothelial cell proliferation, migration, and survival. Phospho-Tyr^{1230}/ Tyr^{1231} directly recruit growth factor receptor-bound protein (GRB2) to VEGFR3, which induces the activation of both AKT and ERK1/2 signaling [26]. In the present study, we also observed concomitant phosphorylation of VEGFR3/AKT/ERK by VEGF-C stimulation and inhibition by aiphanol (Fig. 1d). Our previous study showed that both AKT and MAPKs can be directly inhibited by aiphanol, but this inhibition was rather weak [10]. The observed strong inhibition of AKT and ERK1/2 phosphorylation by aiphanol (Fig. 1d) could result primarily from diminished VEGFR3 phosphorylation. These results further emphasized VEGFR3 as a key target of aiphanol in HDLECs.

We further found that aiphanol downregulated the COX2-dependent secretion of PGE2 and VEGF-C in tumor cells and TAMs, confirming the roles of COX2 in regulating prostaglandin synthesis, VEGF-C expression and lymphangiogenesis in post-partum breast cancer [27, 28]. Additionally, the inhibitory effect of aiphanol on the COX2-PGE2-MMP2/9 axis may prevent tumor cells from invading from the primary lesion to distant sites. These findings demonstrated that aiphanol could modulate the interplay among LECs, tumor cells and macrophages to ultimately inhibit VEGF-C-VEGFR3 signaling, therefore interfering with lymphangiogenesis and lymphatic metastasis.

Considering that the complexity and redundancy of lymphangiogenic network modulation [29], multi-targeting inhibitors may be more suitable candidates for combating tumor-associated lymphangiogenesis and lymphatic dissemination due to their ability to overcome limitation of single-targeting inhibitors, such as their limited potency, unsatisfactory safety and resistance profiles [30–32]. Natural drugs have the characteristic of well-known polypharmacological profile and have recently been assessed as multi-targeting drugs for lymphangiogenesis. For instance, curcumin inhibits capillary-like tube formation of rat lymphatic endothelial cells partially through AKT and MMP-2 [33]. Kaempferol is an inhibitor of VEGFR2/3 kinase activity and reduces the density of tumor-associated lymphatic vessels as well as the incidence of lymph node metastasis in vivo [34]. Phomaketide A, a marine fungus-derived compound, inhibits lymphangiogenesis by decreasing VEGFR3-PKCδ-eNOS signaling and activating protease inhibitors [35]. Resveratrol inhibits lymphangiogenesis and abolishes M2 macrophage activation and differentiation in TAMs to suppress tumor progression [36]. The antitumor and antimetastatic functions of wogonin are closely related to the suppression of lymphangiogenesis through reductions in VEGFR3 activity, COX2 expression and IL-1β production in TAMs [37]. Likewise, our present study showed that aiphanol has some parallels with the above natural remedies in antagonizing lymphangiogenesis, including its ability to inactivate VEGFR3 signaling and alter COX2 and TAMs. We identified mechanisms by which aiphanol

blunts the activity of VEGFR3 and COX2 via direct binding and does not affect the expression of these proteins. COX2 can accelerate M2 macrophage infiltration to increase tumor invasion and can predict poor prognosis [38, 39], while aiphanol decreased M2 macrophage aggregation in the tumor microenvironment, an effect associated with inhibition of COX2 activity. These results indicated that aiphanol has a wealth of potential targets, with superiority over other natural drugs. Therefore, aiphanol might have more application in clinical settings in the future.

Multiple VEGFR inhibitors, for example, fruquintinib [40] and tivozanib [41], are currently available in the clinic. Compared with these VEGFR inhibitors, aiphanol has the following advantages: (i) aiphanol, a less reported natural stilbenolignan, has a novel molecular skeleton [9] and is structurally different from many synthetic VEGFR kinase inhibitors. (ii) As we found, aiphanol directly binds to and suppresses the activity of the cyclooxygenase enzyme COX2 and the tyrosine kinase VEGFR3. To date, there is no inhibitor that can simultaneously inhibit the activity of these two types of enzymes. Therefore, the mechanism by which aiphanol inhibits lymphangiogenesis is well-defined and unique. (iii) Aiphanol can inhibit the activity of a variety of tyrosine kinases and serine/threonine kinases [10]. In addition to its inhibition on VEGFR3, COX2 and VEGFR2, aiphanol exhibited direct, but weak to modest, inhibition on the kinase activity of PI3Ks (PI3K(p110β/p85α), PI3K(p110δ/p85α), PI3K(p110α/p85α), PI3K(p110α/p65α), PI3KC2α and PI3KC2γ). Aiphanol also directly and weakly inhibited the activity of AKT1/PKBα, AKT3/PKBγ and PDK1, while slightly stimulated the activity of AKT2/PKBβ [10]. Thus, several VEGFR3-PI3K-PDK-AKT pathway components could be inhibited by aiphanol. Additionally, aiphanol can moderately inhibit the activity of several members of the MAPK cascade, including ERK1/MAPK3 and ERK2/MAPK1 [10]. These observations may explain why the assays showed that the effects of VEGFR3 knockdown on HDLECs proliferation, tubular formation and motility were weaker than those of aiphanol treatment (Fig. 3h–k, Supplementary Fig. S4a, b), which indicates that, in addition to targeting VEGFR3, other mechanism(s) may also contribute to aiphanol's antilymphangiogenic activity. Furthermore, administration of aiphanol, but not SAR (both at 30 mg/kg), increased the survival time of tumor-bearing mice, likely because the effect of SAR on prolonging the median survival of mice was achieved only at higher dose (100 mg/kg) [8]. This observation also highlights that compared to the single-targeting inhibitor, aiphanol, as a multi-targeting agent, could exhibit satisfactory efficacy even at a lower dose.

Currently, the combination of immunomodulatory agents and multikinase inhibitors [42, 43] provides opportunities for the antitumor immune function of the tumor microenvironment and yields distinctly improved antitumor efficacy. For example, sorafenib, a multikinase inhibitor with activity against VEGFR2/3, PDGFRβ, FLT3 and c-Kit, promoted CD4 positive and CD8 positive T-cell infiltration and enhanced tumor regression [44]. Axitinib, an inhibitor of VEGFR1/2/3 and PDGFRβ, reversed tumor-induced immunosuppression via a decrease in TAM infiltration, and led to a synergistic therapeutic effect in combination with immunomodulatory antibodies [45]. The COX2-PGE2 axis increases PD-L1 expression in myeloid-derived suppressor cells and TAMs in tumors [46]. Dual inhibition of COX2 and EGFR by melafolone enhanced the effect of checkpoint blockade therapy through vascular normalization and PD-L1 downregulation [47]. We demonstrated that aiphanol can simultaneously inhibit the activity of VEGFR3, COX2 and VEGFR2, indicating that it may have the potential to be developed into a novel multi-targeting agent to improve the effects of immune checkpoint blockade therapy for cancer.

In conclusion, our studies shed light on the antilymphangiogenic and antilymphatic metastasis effects of aiphanol, a representative natural stilbenolignan that has been relatively less investigated, in in vivo, ex vivo, and in vitro systems for the first time. Aiphanol was shown to suppress lymphangiogenesis by targeting VEGFR3 cascades and controlling the COX2-PGE2-VEGF-C axis in tumor cells and macrophages. The incidence of LN dissemination was decreased and the median survival of tumor-bearing mice was prolonged when aiphanol was administered via the oral route. Therefore, we propose that aiphanol might be a promising multi-targeting lead compound to mitigate cancer lymphatic metastasis.

ACKNOWLEDGEMENTS

This study was supported by the National Natural Science Foundation of China (81773219), National Basic Research Program of China (2015CB553906), the Digestive Medical Coordinated Development Center of Beijing Hospitals Authority (XXT21, China), Clinical Medicine Plus X - Young Scholars Project, Peking University, the Fundamental Research Funds for the Central Universities (PKU2022LCXQ021) and the PKU-Baidu Fund (2019BD015, China). The author would like to thank Mrs. Hui Xu (Peking University Cancer Hospital & Institute, Beijing, China) for help in animal studies, Dr. Bin Dong (Peking University Cancer Hospital & Institute, Beijing, China) for assistance in frozen sections, and Mrs. Jing Wang (School of Pharmaceutical Sciences, Peking University, Beijing, China) for assistance in SPR and BLI assays.

AUTHOR CONTRIBUTIONS

CCS, LKQ, CKZ and YXJ designed experiments; YXJ and LCY synthesized Aiphanol and biotin-Aiphanol. SMC, LXW, and YNM carried out experiments; SMC, CCS, LKQ and CKZ analyzed experimental results; CCS, LKQ, SMC and CKZ wrote the manuscript; LM and CYL provided laboratory assistance. SQC identified Aiphanol from *Sarsaparilla*.

ADDITIONAL INFORMATION

Supplementary information The online version contains supplementary material available at https://doi.org/10.1038/s41401-022-00940-4.

Competing interests: The authors declare no competing interests.

REFERENCES

1. Steeg PS. Targeting metastasis. Nat Rev Cancer. 2016;16:201–18.
2. Alitalo K. The lymphatic vasculature in disease. Nat Med. 2011;17:1371–80.
3. Dieterich LC, Seidel CD, Detmar M. Lymphatic vessels: new targets for the treatment of inflammatory diseases. Angiogenesis. 2014;17:359–71.
4. Stacker SA, Williams SP, Karnezis T, Shayan R, Fox SB, Achen MG. Lymphangiogenesis and lymphatic vessel remodelling in cancer. Nat Rev Cancer. 2014;14:159–72.
5. Stacker SA, Achen MG, Jussila L, Baldwin ME, Alitalo K. Lymphangiogenesis and cancer metastasis. Nat Rev Cancer. 2002;2:573–83.
6. Wu H, Rahman H, Dong Y, Liu X, Lee Y, Wen A, et al. Epsin deficiency promotes lymphangiogenesis through regulation of VEGFR3 degradation in diabetes. J Clin Invest. 2018;128:4025–43.
7. Burton JB, Priceman SJ, Sung JL, Brakenhielm E, An DS, Pytowski B, et al. Suppression of prostate cancer nodal and systemic metastasis by blockade of the lymphangiogenic axis. Cancer Res. 2008;68:7828–37.
8. Alam A, Blanc I, Gueguen-Dorbes G, Duclos O, Bonnin J, Barron P, et al. SAR, a potent and selective VEGFR-3-TK inhibitor with antilymphangiogenic, antitumoral, and antimetastatic activity. Mol Cancer Ther. 2012;11:1637–49.
9. Lee D, Cuendet M, Vigo JS, Graham JG, Cabieses F, Fong HH, et al. A novel cyclooxygenase-inhibitory stilbenolignan from the seeds of *Aiphanes aculeata*. Org Lett. 2001;3:2169–71.
10. Chen S, Feng J, Zhao C, Wang L, Meng L, Liu C, et al. Aiphanol, a native compound, suppresses angiogenesis via dual-targeting VEGFR2 and COX2. Signal Transduct Target Ther. 2021;6:413.
11. Lala PK, Nandi P, Majumder M. Roles of prostaglandins in tumor-associated lymphangiogenesis with special reference to breast cancer. Cancer Metastasis Rev. 2018;37:369–84.
12. Su JL, Shih JY, Yen ML, Jeng YM, Chang CC, Hsieh CY, et al. Cyclooxygenase-2 induces EP1- and HER-2/Neu-dependent vascular endothelial growth factor-C up-regulation: a novel mechanism of lymphangiogenesis in lung adenocarcinoma. Cancer Res. 2004;64:554–64.
13. Chen C, He W, Huang J, Wang B, Li H, Cai Q, et al. LNMAT1 promotes lymphatic metastasis of bladder cancer via CCL2 dependent macrophage recruitment. Nat Commun. 2018;9:3826.

14. Ji H, Cao R, Yang Y, Zhang Y, Iwamoto H, Lim S, et al. TNFR1 mediates TNF-α-induced tumour lymphangiogenesis and metastasis by modulating VEGF-C-VEGFR3 signalling. Nat Commun. 2014;5:4944.
15. Cao Y. Opinion: emerging mechanisms of tumour lymphangiogenesis and lymphatic metastasis. Nat Rev Cancer. 2005;5:735–43.
16. Lohela M, Saaristo A, Veikkola T, Alitalo K. Lymphangiogenic growth factors, receptors and therapies. Thromb Haemost. 2003;90:167–84.
17. Chang J, Kim Y, Kwon HJ. Advances in identification and validation of protein targets of natural products without chemical modification. Nat Prod Rep. 2016;33:719–30.
18. Jafari R, Almqvist H, Axelsson H, Ignatushchenko M, Lundbäck T, Nordlund P, et al. The cellular thermal shift assay for evaluating drug target interactions in cells. Nat Protoc. 2014;9:2100–22.
19. Arroyo-Crespo JJ, Armiñán A, Charbonnier D, Deladriere C, Palomino-Schätzlein M, Lamas-Domingo R, et al. Characterization of triple-negative breast cancer preclinical models provides functional evidence of metastatic progression. Int J Cancer. 2019;145:2267–81.
20. Dinicola S, Masiello MG, Proietti S, Coluccia P, Fabrizi G, Catizone A, et al. Nicotine increases colon cancer cell migration and invasion through epithelial to mesenchymal transition (EMT): COX-2 involvement. J Cell Physiol. 2018;233:4935–48.
21. Hosono K, Isonaka R, Kawakami T, Narumiya S, Majima M. Signaling of prostaglandin E receptors, EP3 and EP4 facilitates wound healing and lymphangiogenesis with enhanced recruitment of M2 macrophages in mice. PLoS ONE. 2016;11:e0162532.
22. Dieterich LC, Detmar M. Tumor lymphangiogenesis and new drug development. Adv Drug Deliv Rev. 2016;99:148–60.
23. Yang C, Ma C, Li Y, Mo P, Yang Y. High Tiam1 expression predicts positive lymphatic metastasis and worse survival in patients with malignant solid tumors: a systematic review and meta-analysis. Onco Targets Ther. 2019;12:5925–36.
24. Biaoxue R, Xiling J, Shuanying Y, Wei Z, Xiguang C, Jinsui W, et al. Upregulation of Hsp90-beta and annexin A1 correlates with poor survival and lymphatic metastasis in lung cancer patients. J Exp Clin Cancer Res. 2012;31:70.
25. Dixelius J, Makinen T, Wirzenius M, Karkkainen MJ, Wernstedt C, Alitalo K, et al. Ligand-induced vascular endothelial growth factor receptor-3 (VEGFR-3) heterodimerization with VEGFR-2 in primary lymphatic endothelial cells regulates tyrosine phosphorylation sites. J Biol Chem. 2003;278:40973–9.
26. Salameh A, Galvagni F, Bardelli M, Bussolino F, Oliviero S. Direct recruitment of CRK and GRB2 to VEGFR-3 induces proliferation, migration, and survival of endothelial cells through the activation of ERK, AKT, and JNK pathways. Blood. 2005;106:3423–31.
27. Lyons TR, O'brien J, Borges VF, Conklin MW, Keely PJ, Eliceiri KW, et al. Postpartum mammary gland involution drives progression of ductal carcinoma in situ through collagen and COX-2. Nat Med. 2011;17:1109–15.
28. Lyons TR, Borges VF, Betts CB, Guo Q, Kapoor P, Martinson HA, et al. Cyclooxygenase-2-dependent lymphangiogenesis promotes nodal metastasis of postpartum breast cancer. J Clin Invest. 2014;124:3901–12.
29. Tammela T, Alitalo K. Lymphangiogenesis: molecular mechanisms and future promise. Cell. 2010;140:460–76.
30. Matias M, Le Teuff G, Albiges L, Guida A, Brard C, Bacciarelo G, et al. Real world prospective experience of axitinib in metastatic renal cell carcinoma in a large comprehensive cancer centre. Eur J Cancer. 2017;79:185–92.
31. Duerinck J, Du Four S, Bouttens F, Andre C, Verschaeve V, Van Fraeyenhove F, et al. Randomized phase II trial comparing axitinib with the combination of axitinib and lomustine in patients with recurrent glioblastoma. J Neurooncol. 2018;136:115–25.
32. Kanwar SS, Yu Y, Nautiyal J, Patel BB, Padhye S, Sarkar FH, et al. Difluorinated-curcumin (CDF): a novel curcumin analog is a potent inhibitor of colon cancer stem-like cells. Pharmacol Res. 2011;28:827–38.
33. Matsuo M, Sakurai H, Koizumi K, Saiki I. Curcumin inhibits the formation of capillary-like tubes by rat lymphatic endothelial cells. Cancer Lett. 2007;251:288–95.
34. Astin JW, Jamieson SM, Eng TC, Flores MV, Misa JP, Chien A, et al. An in vivo antilymphatic screen in zebrafish identifies novel inhibitors of mammalian lymphangiogenesis and lymphatic-mediated metastasis. Mol Cancer Ther. 2014;13:2450–62.
35. Tai HC, Lee TH, Tang CH, Chen LP, Chen WC, Lee MS, et al. Phomaketide A inhibits lymphangiogenesis in human lymphatic endothelial cells. Mar Drugs. 2019;17:215.
36. Kimura Y, Sumiyoshi M. Resveratrol prevents tumor growth and metastasis by inhibiting lymphangiogenesis and M2 macrophage activation and differentiation in tumor-associated macrophages. Nutr Cancer. 2016;68:667–78.
37. Kimura Y, Sumiyoshi M. Anti-tumor and anti-metastatic actions of wogonin isolated from Scutellaria baicalensis roots through anti-lymphangiogenesis. Phytomedicine. 2013;20:328–36.
38. Xu J, Yu Y, He X, Niu N, Li X, Zhang R, et al. Tumor-associated macrophages induce invasion and poor prognosis in human gastric cancer in a cyclooxygenase-2/MMP9-dependent manner. Am J Transl Res. 2019;11:6040–54.
39. Chen EP, Markosyan N, Connolly E, Lawson JA, Li X, Grant GR, et al. Myeloid cell COX-2 deletion reduces mammary tumor growth through enhanced cytotoxic T-lymphocyte function. Carcinogenesis. 2014;35:1788–97.
40. Li J, Qin S, Xu RH, Shen L, Xu J, Bai Y, et al. Effect of fruquintinib vs placebo on overall survival in patients with previously treated metastatic colorectal cancer: The FRESCO Randomized Clinical Trial. JAMA. 2018;319:2486–96.
41. Rini BI, Pal SK, Escudier BJ, Atkins MB, Hutson TE, Porta C, et al. Tivozanib versus sorafenib in patients with advanced renal cell carcinoma (TIVO-3): a phase 3, multicentre, randomised, controlled, open-label study. Lancet Oncol. 2020;21:95–104.
42. Sharma P, Allison JP. Immune checkpoint targeting in cancer therapy: toward combination strategies with curative potential. Cell. 2015;161:205–14.
43. Melero I, Berman DM, Aznar MA, Korman AJ, Pérez Gracia JL, Haanen J. Evolving synergistic combinations of targeted immunotherapies to combat cancer. Nat Rev Cancer. 2015;15:457–72.
44. Sunay MM, Foote JB, Leatherman JM, Edwards JP, Armstrong TD, Nirschl CJ, et al. Sorafenib combined with HER-2 targeted vaccination can promote effective T cell immunity in vivo. Int Immunopharmacol. 2017;46:112–23.
45. Läubli H, Müller P, D'Amico L, Buchi M, Kashyap AS, Zippelius A. The multi-receptor inhibitor axitinib reverses tumor-induced immunosuppression and potentiates treatment with immune-modulatory antibodies in preclinical murine models. Cancer Immunol Immunother. 2018;67:815–24.
46. Prima V, Kaliberova LN, Kaliberov S, Curiel DT, Kusmartsev S. COX2/mPGES1/PGE2 pathway regulates PD-L1 expression in tumor-associated macrophages and myeloid-derived suppressor cells. Proc Natl Acad Sci USA. 2017;114:1117–22.
47. Tang H, Liu Y, Wang C, Zheng H, Chen Y, Liu W, et al. Inhibition of COX-2 and EGFR by melafolone improves anti-PD-1 therapy through vascular normalization and PD-L1 downregulation in lung cancer. J Pharmacol Exp Ther. 2019;368:401–13.